Applied Catalysis B: Environmental 203 (2017) 807–819

Contents lists available at ScienceDirect

Applied Catalysis B: Environmental

journal homepage: www.elsevier.com/locate/apcatb

# *In-situ* catalytic upgrading of heavy oil using dispersed bionanoparticles supported on gram-positive and gram-negative bacteria

Jacob B. Omajali[a,1], Abarasi Hart[b], Marc Walker[c], Joseph Wood[b], Lynne E. Macaskie[a,*]

[a] Unit of Functional Bionanomaterials, Institute of Microbiology and Infection, School of Biosciences, University of Birmingham, Edgbaston, Birmingham B15 2TT, United Kingdom
[b] School of Chemical Engineering, University of Birmingham, Edgbaston, Birmingham, B15 2TT, United Kingdom
[c] Department of Physics, University of Warwick, Coventry, CV4 7AL, United Kingdom

ARTICLE INFO

*Article history:*
Received 9 July 2016
Received in revised form 22 October 2016
Accepted 26 October 2016
Available online 28 October 2016

*Keywords:*
Bio-nanoparticles
Coking
Heavy oil
Upgrading
Viscosity

ABSTRACT

With the continuous depletion of global oil reserves, unconventional alternative oil resources like heavy oil and bitumen have become increasingly attractive. This study investigates the use of bimetallic bio-nanoparticles (bio-NPs), a potential alternative to commercial catalysts in heavy oil upgrading. The bio-NPs were made by sequential reduction of precious metal (Pd and Pt) ions with hydrogen as the electron donor at 5 wt% and 20 wt% metal loading using bacterial (*Desulfovibrio desulfuricans* and *Bacillus benzeovorans*) cells as support. The bio-NPs were characterized using transmission electron microscopy (TEM), X-ray powder diffraction (XRD) and X-ray photoelectron spectroscopy (XPS). Results of the catalytic upgrading of a feed heavy oil show that the bimetallic bio-NPs produced an increment of ~2° in API (American Petroleum Institute) gravity (*i.e.* ~9.1°) better than monometallic bio-NPs (~7.6°) on average while the API gravity using thermal upgrading was lower (6.3°). The API gravity of a commercial Ni-Mo/$Al_2O_3$ catalyst was 11.1°. However, more coking was produced using the commercial catalyst than with the bio-NPs. The extent of viscosity reduction was: 98.7% (thermal), 99.2% (bio-NPs) and 99.6% (Ni-Mo/$Al_2O_3$) below 1031 mPa s for the feed heavy oil reference (baseline). The potential advantage of using bio-NPs is that the precious metals can be sourced cheaply from waste streams, which could serve as a potential platform for the green synthesis of catalytically active materials using bacteria for *in-situ* catalytic upgrading of heavy oils.



## 1. Introduction

The world's energy consumption has been projected by the US Energy Information Administration (EIA) to reach approximately $8.6 \times 10^6$ joules per annum by 2040 [1]. Oil, the world's leading fuel source, supports 32% of global energy consumption, which increased by 2.3% in 2013 [2]. It has been reported that most of the future energy demand will be dominated (95%) by the non-OECD (non-Organization for Economic Cooperation and Development) countries where demand is driven by strong economic growth [2]. As consumption of world energy continues to rise, fossil fuels are expected to remain the predominant sources of supply, satisfying about 80% of global needs [3] despite major concerns about environmental consequences.

A consequence of the increase in demand and consumption of light crude oil is a global decline in reserves and supply. Therefore, there is a need to supplement short-and-long term needs through less conventional oil resources, like heavy oil and bitumen, whose current production stands at 2–3% (2 million barrels/day, Mb/d) of global supply, with output predicted to reach 7 Mb/d in 2030 [4]. Large deposits of heavy oil and bitumen occur in locations such as Canada (the Alberta Basin) and Venezuela (the Orinoco Belt), which together comprise about 80% of world's remaining oil reserves [5]. Substantial deposits of heavy oil are also located in the Middle East, although owing to its vast light oil reserves, documentation of these reserves tends to be incomplete [6]. Exploitation of these heavy oils forms a major challenge due to their inherent properties *i.e.* high viscosity, low hydrogen content, presence of high molecular weight compounds (resins and asphaltenes) and rich-

* Corresponding author.
*E-mail address:* L.E.Macaskie@bham.ac.uk (L.E. Macaskie).
[1] Current address: Department of Biological Sciences, Faculty of Sciences, Thompson Rivers University, 900 McGill Road, V2C 0C8, Kamloops, British Columbia, Canada.

http://dx.doi.org/10.1016/j.apcatb.2016.10.074

ness in hetero-elements (nitrogen, sulfur and oxygen), as well as high metal contents, especially nickel and vanadium. These properties of heavy oil are thought to be the consequence of subsurface water flows and also microbial activities within a shallow depth of low temperature environments as the oil accumulates over time [7]. Microbial processes introduce changes, especially in the light end of the oil, specifically the hydrocarbon molecules (oxidation of $C_{6+}$ components), leading to fluids characterized by high contents of heavy molecules rich in sulfur, nitrogen, oxygen and metals but with decreased API gravity and increased viscosity and acidity [7,8]. Other challenges include environmental concerns such as water management, specifically production water for steam generation, and the control of greenhouse gases and other pollutants during the extra refining required for heavy oils [8].

*In-situ* upgrading technologies such as catalytic thermal conversions in the presence of hydrogen, hydrogen donor solvents and the use of microbial communities generating methane (biodegradation of $C_2$-$C_5$ hydrocarbons) are currently in use but not yet at industrial scale [9] coupled with other emerging technologies [10] which all have environmental advantages because of their ability to trap most of the pollutants generated from heavy oil in the reservoir well. They also reduce the need for surface upgrading, which results in the cleaner production of lower viscosity oil, which is more easily transported without the use of diluents. The THAI-CAPRI (Toe-to-Heel Air Injection coupled with Catalytic Upgrading Process *In-situ*) technology combines thermally enhanced oil recovery with downhole *in-situ* catalytic upgrading of heavy oil into light fractions [11–13]. This technology, shown for the *in-situ* catalytic upgrading of heavy oil in the presence of steam, hydrogen and methane has demonstrated significant improvements over non-catalytic thermal processes [17].

However commercial cracking catalysts such as noble metals on chemical supports are prohibitively expensive for a large scale once-through technology; an alternative source of cheaper catalyst is therefore essential. One of the options is to utilize regenerated catalysts from treated oils as reported previously [12] which could reduce catalyst cost but the disadvantage is in their low activity. The emergent use of bacteria as new systems for catalyst manufacture [14] provides alternative sources for patterning of metallic nanoparticles (NPs) called bio-nanoparticles (bio-NPs) which are held supported on the cells as micron-sized carriers. Advantages of using bacteria include scalability of NP synthesis, non-toxic reducing agents and supports when compared to strong toxic chemical reductants used in commercial systems and as remediation platforms for precious metal-containing wastes [15]. In addition, the various functional groups (amine, carboxyl, hydroxyl, sulfuryl and phosphoryl) found on bacterial cell surfaces, tend to control and stabilize particle growth [16] *via* 'bio-patterning' as compared to the use of surfactants and capping agents which introduce artefacts into commercial catalysts. In some cases metallic bio-NPs biorefined from wastes can have higher activity than monometallic bio-NPs [17]. When biomanufactured from an otherwise discarded source such as road dust the concept of a 'once-through' loss into the environment becomes conceptually and economically acceptable and this forms the goal of this investigation. This is because platinum group metals (PGMs – Pd, Pt and Ru) recovered from secondary sources can be bio-converted using bacterial cells (obtainable as wastes from fermentation process and industrial enzyme and drug production) into useful PGM catalysts with various industrial and environmental applications [18]. Recovery from waste streams would reduce the cost of catalyst production and the attendant environmental concerns, especially with regards to the high energy demands required in conventional mining technology. The quantity of PGMs recovered from wastes and through bioconversion by bacterial cells are usually below current economic standard values but this is regarded as an environmentally sustainable approach with the possibility of future improvement in the process *via* waste upgrading [19]. In addition, the economic reality of using PGM catalysts in catalytic conversion has been highlighted previously [20] and by the authors in a recent paper [21].

The use of *Desulfovibrio desulfuricans* (Gram-negative) and *Bacillus* sp. (Gram-positive) bacteria has been widely examined in the context of bio-NPs catalyst production [22–24]. However, the production of hydrogen sulfide (normally a strong catalyst poison) by the former, coupled with the problem of production at scale, would make *Bacillus* more preferable but on the other hand, sulfidation of metals by sulfur often leads to activation of catalyst [25]. In spite of various reports about the poisoning effects of sulfur-containing species on precious metal catalysts [26,27], the adsorption of sulfur onto the surface of heterogeneous metal catalyst (including PGM catalysts) at very low concentrations was reported to influence various catalytic properties such as promotion of activity and enhancement of selectivity [27,28] and sometimes prolongs the life-span of PGM catalysts [26]. Interestingly, recent work [29,30] has shown *via* high resolution transmission electron microscopy and elemental mapping the ability of palladium nanoparticles to co-localize with bacterial sulfhydryl groups, an effect which may result in partial poisoning or elongation of the life-span of a PGM catalyst. *Bacillus* spp. are produced in large quantities *via e.g.* the commercial manufacturing of enzymes and hence waste biomass could provide a sustainable source for the synthesis of new catalytic materials.

Various precious metals (*e.g.* Pd, Pt and Au) have been reductively precipitated into bio-NPs by various strains of Gram-negative and Gram-positive bacteria and utilized in a range of catalytic reactions of industrial importance, with activities comparable to commercial catalysts [31,32]. Some of these important reactions of bio-NPs made *via* reduction at the expense of either hydrogen or formate include the reductive dechlorination of polychlorinated biphenyls [33,34], chromium VI reduction [15,35] and dehalogenation of dichlofenac [36]. Similar synthetic approaches have been used to produce bio-NPs with relevance in the pharmaceutical industries particularly in Heck-coupling and Suzuki reactions [32,24] while Zhu et al. [37] demonstrated their applications in selective hydrogenation of 2-pentyne and soy bean oil. In addition, bio-NPs synthesized from the plant, *Arabidopsis* was used as a heterogeneous catalyst in a Suzuki reaction [38] while bio-NPs made from fungal mycelia degraded 4-nitrophenol [39]. More recently, a silver bio-NP nanocluster with luminescent properties was developed with the ability to bind to tumor cells [40]. Meanwhile there are no reports on the use of bimetallic bio-NPs for *in-situ* catalytic upgrading of heavy oil prior to this study; metallic mixtures would be the unavoidable characteristic of a bio-catalyst made from a waste with little or no metal selectivity in the biorecovery step [14]. It was reported that bimetallic bio-NPs are more catalytically active in various reactions than their monometallic counterparts [36], attributed to the synergistic effects of the two metals, which has also been shown in chemical synthesis [41]. For example, a bio-Pd/Au core-shell bimetallic catalyst synthesized using *E-coli* was shown to be comparable to a commercial catalyst in the selective oxidation of benzyl alcohol [42] while De Corte et al. [36] synthesized Pd/Au bimetallic using *S. oneidensis* MR-1 to make a better dechlorination catalyst of dichlofenac than monometallic bio-Pd.

This study evaluates the potential for use of bio-NPs for the upgrading of heavy oil and compares the efficacy of the bio-NPs synthesised on *Desulfovibrio desulfuricans* (bio-$Pd_{Dd}$) with counterparts synthesised on *Bacillus benzeovorans* (bio-$Pd_{Bb}$). Other catalytic tests have shown some strain-dependent differences using monometallic NPs following differences shown between Gram-negative and Gram-positive supports [23]. Hence, the second aim, prerequisite to the biomanufacturing of active bimetallic Pd/Pt NPs from wastes [43] is to compare bimetallic bio-NPs of two

**Table 1**
Properties and composition of heavy oil used in this study.

| Parameter | Value |
|---|---|
| API gravity (°) | 13.8 |
| Viscosity at 20 °C (mPa.s) | 1031 |
| Sulfur (wt.%) | 3.52 |
| Nickel (ppm) | 41 |
| Vanadium (ppm) | 108 |
| Ni + V (ppm) | 149 |
| Asphaltene (wt.%) | 10.3 |
| Elemental analysis | |
| C | 88.82 wt.% |
| H | 10.17 wt.% |
| N | 0.57 wt.% |
| H/C | 0.114 |

Data provided by Touchstone Exploration Inc.

different bacteria with those made using Pd alone. The efficacy of monometallic palladium catalysts in the upgrading of heavy oil, providing a platform for the application of bimetallic PGM catalysts in heavy oil upgrading has recently been shown [21,29] by the authors. For realistic application in a 'once through' process a catalyst biorefined from waste would be bimetallic or even multimetallic and hence even if bimetallics and monometallics perform similarly the way is open for biorefining of a catalyst from waste into greener procurement of heavy oil and hence a more efficient utilization of this fossil resource.

## 2. Experimental

### 2.1. Materials

The heavy oil feedstock used in this study was recovered from oil sands at Kerrobert, Saskatchewan by THAI and was provided by Touchstone Exploration Inc, Canada. Since the feedstock was produced by the THAI process, it was partially upgraded by pyrolysis and its properties are shown in Table 1. A commercial catalyst (NiMo/$Al_2O_3$) was supplied by Akzo Nobel (Amsterdam, Netherlands) with metal loading of 17.4 wt% Mo and 1.8 wt% Ni (19.2 wt% total metal).

### 2.2. Bacterial strains and growth conditions

*Bacillus benzeovorans* NCIMB 12555 (Bb) (aerobic) and *Desulfovibrio desulfuricans* NCIMB 8307 (Dd) (anaerobic) were grown as follows: *B. benzeovorans* was grown aerobically [30] in a rotary shaker (180 rpm at 30 °C) in nutrient medium (pH 7.3 ± 0.2) comprising (per litre) 1.0 g beef extract (Sigma-Aldrich), 2.0 g yeast extract (Sigma-Aldrich), 5.0 g peptone (Sigma-Aldrich) and 15.0 g NaCl. *D. desulfuricans* was grown anaerobically under oxygen-free nitrogen (OFN) in Postgate's medium C [24] (pH 7.5 ± 0.2) at 30 °C (inoculated from a 24 h pre-culture, 10%v/v) in sealed anaerobic bottles without shaking. Bacterial cells were harvested by centrifugation (9094 × *g*, 15 min, 4 °C) at mid exponential growth phase ($OD_{600}$ 0.7–1.0 and $OD_{600}$ 0.5–0.7 respectively) washed three times in air with 20 mM MOPS (morpholinopropanesulfonic acid)-NaOH buffer, pH 7.0 and then concentrated in a small amount of the same buffer [44] and stored at 4 °C under OFN (oxygen-free nitrogen) until use, within 24 h. Bacterial density (mg/ml) was calculated from the $OD_{600}$ *via* a previously determined calibration.

### 2.3. Preparation of bionanoparticles (bio-NPs)

The resting cell suspensions (as above) were transferred into a degassed solution of 2 mM $Na_2PdCl_4$ (Sodium tetrapalladate (II)) salt adjusted to pH 2 with 0.01 M $HNO_3$ and left for biosorption (30 min, 30 °C) to make a monometallic (5 wt%Pd and 20 wt%Pd) bio-NPs. This was achieved by bubbling hydrogen through a Pd (II)-supplemented cell suspension for 15 min as above and then saturating the mixture (in a closed bottle) for an additional 15 min for reduction to reach completion (confirmed by assay of the residual solution [29,30]). The bimetallic Pd/Pt catalysts were prepared by, first reduction of 2 mM Pd (II) solution as above to give bio-Pd. This was harvested centrifugally (no catalyst is lost in recovery [32]), washed twice with distilled water and then resuspended in water based on the method of Deplanche et al. [42] for Pd/Au synthesis with slight modifications, *i.e.* by the addition of 1 mM $K_2PtCl_6$ (potassium hexachloroplatinate (IV)) salt solution to a final metal loading of 5 wt% (2.5 wt%Pd/2.5 wt% Pt) and 20 wt% (10 wt%Pd/10wt%Pt) controlled by 'bio-patterning' on bacterial cells as a result of the various functional groups serving as stabilizers [29]. The content was purged with hydrogen for 15 min and left for 1 h (180 rpm, 30 °C) for reduction. The removal of residual Pd (II) and Pt (IV) from solution was confirmed according to a method previously described [44]. The final bio-catalysts (Bio-Pd and BioPd/Pt) were then washed three times (9094 × *g*, 4 °C, 15 min) with distilled water and once in acetone, dried and then ground by hand for characterization and catalysis.

### 2.4. Characterization of bio-NPs

#### 2.4.1. Transmission electron microscopy

Bio-NPs-loaded cells (bio-Pd/Pt) of *B. benzeovorans* and *D. desulfuricans* were washed twice with distilled water, fixed with 2.5% (w/v aq) glutaraldehyde in 0.1 M cacodylate buffer (pH 7.0) at 4 °C and stained with 1% osmium tetraoxide. The cells were dehydrated using an ethanol series, washed twice in propylene oxide [44], embedded in epoxy resin, cut into sections (100–150 nm thick) and viewed with a JEOL 1200EX transmission electron microscope, accelerating voltage of 80 kV.

#### 2.4.2. X-ray powder diffraction

X-ray powder diffraction (XRD) patterns of samples (bio-NPs) were acquired from a Bruker AXS D8 Autosampler (Transmission) Diffractometer using a monochromatic high-intensity $CuK_{\alpha 1}$ radiation (λ = 1.5406 Å) equipped with a solid-state LynxEye position sensitive detector (PSD) with a 3° electronic window. The XRD patterns were then compared to a reference standard from the International Committee for Diffraction Data (ICDD) database and the crystallite size of the bio-NPs was determined using Scherrer's equation [45].

#### 2.4.3. X-ray photoelectron spectroscopy

Surface chemical composition and oxidation state analysis of bio-Pd/Pt were analyzed using X-ray photoelectron spectroscopy (XPS). Data were collected using a Sphera electron analyzer (Omicron Nanotechnology), with the core levels recorded using a pass energy of 10 eV (resolution approx. 0.47 eV). Due to the insulating nature of the samples, a CN10 charge neutralizer (Omicron Nanotechnology) was used in order to prevent surface charging. A low energy (typically 1.5 eV) beam of electrons was directed on to the sample during XPS data acquisition. Measurements were made at room temperature and at a take-off angle of 90°, allowing a maximum probing depth of approximately 5–10 nm to evaluate bio-NPs bound to the outermost cell surfaces. The data generated were converted into VAMAS format and analyzed using the CasaXPS package [46] employing Shirley backgrounds, mixed Gaussian-Lorentzian (Voigt) lineshapes and asymmetry parameters where appropriate. All binding energies were calibrated to the C 1s peak originating from C—H or C—C groups at 284.6 eV.

### 2.5. Catalytic upgrading of heavy oil

The catalytic activity of the bio-NPs and commercial catalyst was tested in a stirred batch reactor (100 mL capacity, Baskerville, United Kingdom) using 15 g of heavy oil as feedstock. The optimum reaction temperature was used based on previous investigations using a fixed-bed of pelleted commercial catalysts [47,48] with an optimum reaction condition in this work of 30 min at 425 °C, stirring speed of 500 rpm and nanoparticles-to-oil ratio of 1 mg/g as reported by Hart et al. [49] with an initial heat-up-time (~2 h 15 min). The gas atmosphere was nitrogen with initial pressure of 20 bar which increases with the ramp temperature rise (~20–425 °C over 135 min, heating curve given in [21]) and the added gas from the cracking reactions to 74–80 bar (during cooling the pressure decreases to 24–26 bar). A detailed experimental procedure can be found in Hart et al. [49]. In order to evaluate the effect of the bioNP catalyst, experiments were conducted in parallel without bioNPs (thermal cracking only) and also with bacterial biomass (without metals) as controls.

### 2.6. Product analysis

The products of the upgrading reaction consist of light oil (*i.e.*, liquid), non-condensable gas and coke. The produced coke was determined as a percentage of the deposit after reaction using a thermogravimetry (TG) (NETZSCH-Geratebau GmbH, TG 209 F1 Iris®). The thermogravimetric analysis (TGA) was carried out with a ramp temperature increase from 25 to 900 °C under air flow of 50 mL/min. The composition of the produced gas was determined using an Agilent 7890A gas chromatograph. The liquid product (*i.e.* upgraded oil samples) was collected; measurements of viscosity were made as previously described [12,50] (Advanced Rheometer AR1000, TA Instruments), API gravity (portable density meter DMA 35, Anton Paar, UK) and the true boiling point (TBP) (by simulated distillation using an Agilent 6850N Network gas chromatograph in accordance with the ASTM-2887D method; the Agilent 6850N was calibrated using a mix containing $C_5$ to $C_{40}$). The asphaltene content before and after the reactions was determined through precipitation using *n*-$C_7H_{16}$. A detailed description of these analytical procedures was reported elsewhere [12,50]. Fig. 1 summarizes the experimental and analytical methods used in this study.

### 2.7. Product distribution

The mass balances of the three products *i.e.*, liquid, gas, and coke were calculated as percentage of the mass of feed oil into the reactor using Eqs. (1) and (2):

$$\text{Yield (wt.\%)} = W_i/W_F \times 100 \quad (1)$$

$$\text{Yield of gas(wt\%)} = (W_F - W_A)/W_F \times 100 \quad (2)$$

Where $W_i$ is the weight of component i and $W_F$ is the weight of the feed oil (heavy oil fed into the reactor) and $W_A$ is weight of autoclaved content after reaction.

## 3. Results and discussion

### 3.1. Characterization of bio-NPs

#### 3.1.1. Examination by transmission electron microscopy (TEM)

Analysis by TEM of selected samples [5 wt% (2.5%Pd/2.5%Pt) and 20 wt% (10%Pd/10%Pt) bimetallic bio-Pd/Pt] produced by *B. benzeovorans* (Bb) and *D. desulfuricans* (Dd) is shown in Fig. 2. With 5 wt% bio-Pd/Pt produced by the two bacteria, TEM showed more nanoparticles (NPs) distributed within the intracellular matrix in *B. benzeovorans* (Fig. 2a) than in *D. desulfuricans* where no discrete intracellular NPs were visible (Fig. 2b); however most of the NPs formed an electron opaque 'shell' around both types of cell with agglomerates of bio-NPs in *D. desulfuricans* (Fig. 2d) which were found mostly on the surface or periplasmic space of the bacteria.

**Table 2**
Average Pd crystallite size of bio-NPs analysed using XRD.

| Catalyst type | Crystallite size (nm)Bb | Dd |
|---|---|---|
| 5% bio-Pd | 5.10 ± 1.10 | 3.34 ± 0.10 |
| 20% Bio-Pd | 7.45 ± 0.71 | 13.15 ± 1.51 |
| 5% bio-Pd/Pt | 21.16 ± 8.84 | 13.97 ± 0.17 |
| 20% bio-Pd/Pt | 28. 87 ± 4.78 | 16.25 ± 3.10 |

Bb: *Bacillus benzeovorans*; Dd: *Desulfovibrio desulfuricans.* Results are Mean ± SEM, n = 3.

#### 3.1.2. Examination by X-ray powder diffraction (XRD)

XRD analysis (Fig. 3, Table 2) was used to determine the average Pd and Pd/Pt crystallite size of synthesised mono-and bi-metallic bio-NPs (as dry powders) produced by *B. benzeovorans* and *D. desulfuricans* using Scherrer's equation [45]. The XRD powder patterns of 5 wt% monometallic Pd in both organsims showed only amorphous materials (Fig. 3a) while at 20 wt% Pd the characteristic emission peaks of Pd at 2θ approx. = 40.1°, 46.7°, 68.2°, 82.1°, 86.6 (Fig. 3b) were clearly visible with broader peaks in Bio-$Pd_{Bb}$. At 5 wt% (Fig. 3c) of the bimetallic (i.e 2.5%Pd/2.5%Pt) crystalline Pd/Pt was apparent in Bb only while Dd showed only amorphous Pd/Pt. However, at a higher loading of 20 wt% (10%Pd/10%Pt) both cell types gave clearly defined patterns which were crystalline (Fig. 3d). The Pd peaks at 2θ approx. = 40.1°, 46.7°, 68.2°, 82.1°, 86.6° in both mono and bimetallic bio-NPs corresponds to the lattice planes; (111), (200), (220), (311) and (222) which is consistent with a previous report [51] and a face cubic centre (fcc) crystal structure [52] and the Pt peaks in the bimetallic appeared at 2θ approx. = 39. 93°, 46.3°, 67.7°, 81.46° and 85.9° with the same lattice planes as those in Pd except for 5 wt% bio-Pd/Pt NPs by *D. desulfuricans* and 5 wt% bio-Pd made by both bacteria where only one prominent peak at 2θ = 39.8° or 40.1° (attributed to the (111) plane) was present, in accordance with the ICDD database.

Overall, the monometallic Pd (111) and bimetallic Pd-Pt (111) lattice planes at 40.1° and 39.93°, respectively displayed the strongest diffraction peaks (Fig. 3) indicating high crystallinity [53] with the exceptions of 5 wt% bimetallic Pd/Pt made by *D. desulfuricans* (Fig. 3c) and the 5 wt% monometallic Pd made by both bacteria (Fig. 3a). The average crystallite size was calculated from the Scherrer equation:

$$D = 0.9\lambda/\beta\cos\theta, \quad (3)$$

Where D is the crystallite size in Å, λ is the X-ray wavelength, $CuK_{\alpha 1}$ radiation (λ = 1.5406 Å), $\theta$ is the Bragg angle, and $\beta$ is the full width at half maximum (fwhm, in radians) of the peaks considered.

The average crystallite sizes calculated using Eq. (3) for the bimetallic Pd/Pt (5 wt% and 20 wt%) made by *B. benzeovorans* were generally larger than those produced by *D. desulfuricans* (Table 2) with the exception that the average crystallite size of the 20 wt% monometallic Pd-NPs produced by *B. benzeovorans* was smaller (7.45 ± 0.71 nm) than *D. desulfuricans* (13.15 ± 1.15 nm) but were larger than the corresponding 5% monometallic Pd-NPs respectively (Tables 3a and 3b). Using combined imaging and surface probing techniques, Deplanche et al. [42] reported a size of 16 nm for 5 wt% Pd/Au bimetallic NPs synthesized using *E.coli*. In a previous study [42] on the formation of Pd/Au core-shell bionanoparticles (Au core/Pd shell) the initial Pd-deposit (crystalline) became amorphous when the bimetallic was formed, consistent with migration of Pd atoms to form a shell around the Au core [42]. In this case reduction of Au (III) was mediated by Pd (0) under $H_2$. It is not known in the present case whether reduction of Pt (IV) was

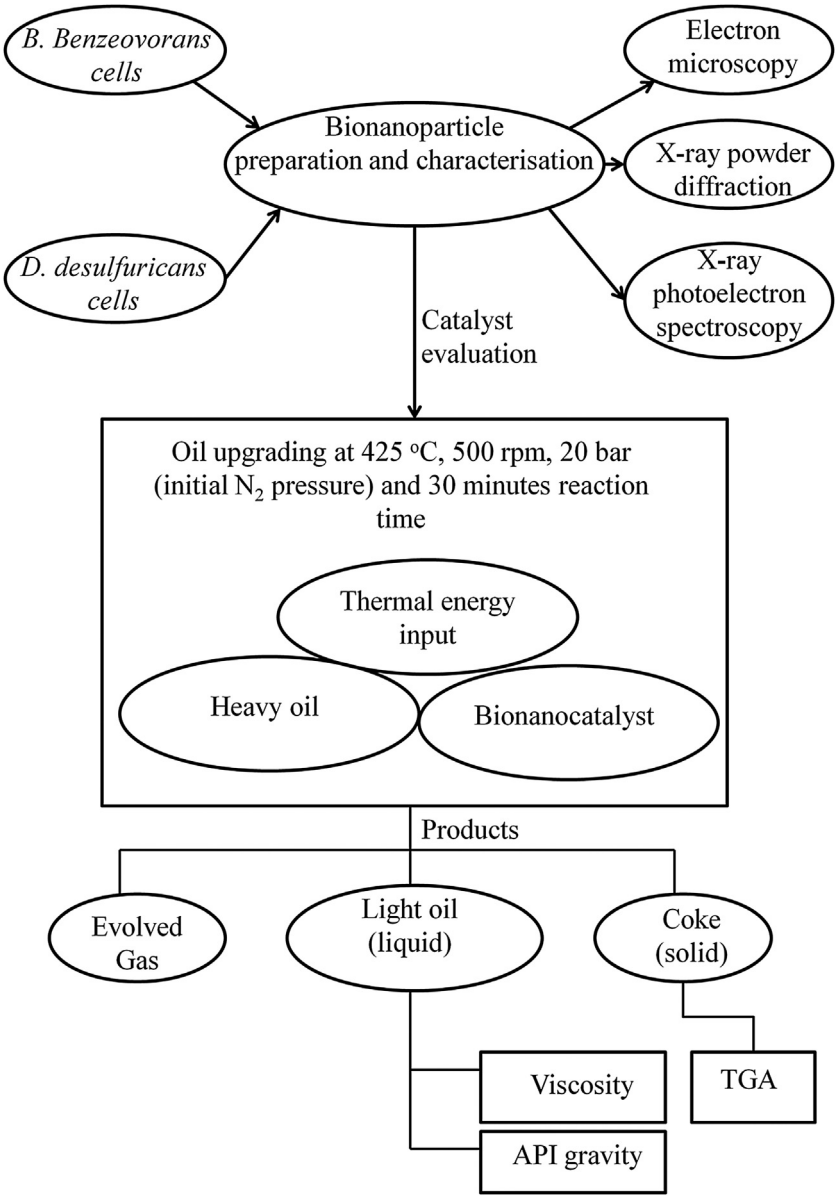


**Fig. 1.** An overview of experimental methods. TGA: Thermogravimetric analysis. API gravity: American petroleum institute gravity (a standard reference for measuring the quality of oil and transportability).

**Table 3a**
XPS binding energies of bio-Pd/Pt bimetallic bio-NPs.

| Bimetallic bio-NPs | Pd $3d_{5/2}$ BE (eV) Bb Dd | | Pt $4f_{7/2}$ BE (eV) Bb Dd | | Pt $4f_{5/2}$ BE (eV) Bb Db | |
|---|---|---|---|---|---|---|
| 5 wt% | 335.23 | 335.55 | – | – | – | – |
| bio-Pd/Pt | 337.69 | 337.42 | | | | |
| 20 wt% | 335.72 | 335.17 | 72.04 | 71.28 | 75.37 | 74.61 |
| bio-Pd/Pt | 337.62 | 337.26 | 72.90 | 72.14 | 76.23 | 75.47 |

XPS binding energies of palladium and platinum bimetallic bio-NPs made by *B. benzeovorans* (Bb) and *D. desulfuricans* (Dd) indicating the presence of Pd $3d_{5/2}$ and Pt 4f doublets. BE = Binding energy of electrons.

**Table 3b**
XPS elemental fractions of bio-Pd/Pt.

| Bimetallic bio-NPs | N1s BE (eV) Bb Dd | | P2p BE (eV) Bb Dd | | O1s BE (eV) Bb Dd | |
|---|---|---|---|---|---|---|
| 5 wt% | 399.72[a] | 399.68[a] | 133.22 | 133.99 | 531.20 | 531.02 |
| bio-NPs | 401.50[b] | 401.59[b] | 134.08 | 134.85 | 532.34 | 532.49 |
| 20 wt% | 399.68[a] | 399.54[a] | 133.72 | 133.96 | 530.98 | 530.81 |
| bio-NPs | 401.61[b] | 401.64[b] | 134.62 | 134.82 | 532.43 | 532.39 |

XPS binding energies of elemental fractions; N1s, P 2p and O1 s of bimetallic bio-NPs. Details of the C1s component is presented in Table S2 and Fig. S3.

[a] Non-protonated nitrogen group.

[b] Protonated nitrogen group; Bb = *Bacillus benzeovorans;* Dd = *Desulfovibrio desulfuricans;* BE = Binding energy of electrons.

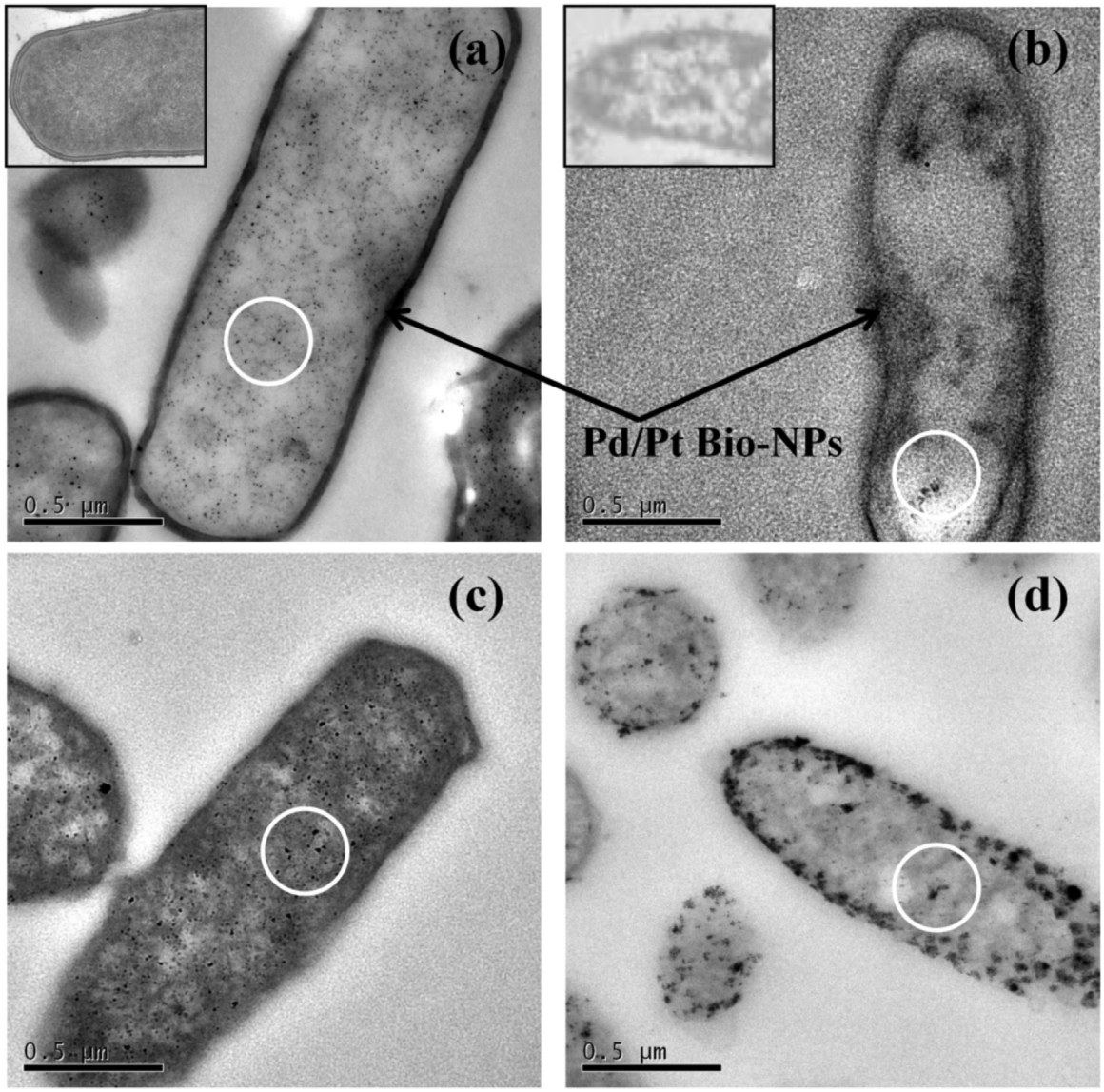


**Fig. 2.** TEM images of 5 wt% bimetallic bio-NPs made by a) B. *benzeovorans* and b) *D. desulfuricans* with corresponding 20 wt% bimetallic bio-NPs c) and d) respectively. Scale bar is 0.5 µm. Insets are cells with no metals. Intracellular NPs are circled.

mediated chemically (*via* Pd (0) 'seed') or enzymatically but the XRD patterns (Fig. 3c and d) clearly demonstrate the existence of Pt NPs. Note that XRD is a 'bulk' characterization technique and hence the values reported in Table 2 represent both surface-localized and intracellular NPs, and no attempt was made to distinguish between them. However one notable difference between the two cell types is that with *D.desulfuricans* no crystalline features were apparent in either the monometallic or bimetallic 5 wt% preparation (Fig. 3a) whereas the bimetallic promoted formation of a crystalline deposit in *B. benzeovorans* which was absent from its counterpart in *D. desulfuricans* (Fig. 3c). This suggests differences between the two biomass types that will be discussed in a subsequent publication.

### *3.1.3. Examination of surface NPs by X-ray photoelectron spectroscopy*

In order to determine the surface chemical composition of bio-NPs and the oxidation states of the resulting Pd/Pt, X-ray photoelectron spectroscopy (XPS) was used to analyze the bimetallic bio-NPs (5 wt% and 20 wt% bio-Pd/Pt). Fig. 4 and Table 3a show the XPS spectra of Pd 3d and Pt 4f for Pd and Pt respectively present on the surface of the bio-NPs. There are two oxidation states for both Pd and Pt in the bio-NPs as shown by two binding energy doublets. For 5 wt% and 20 wt% bio-Pd/Pt bimetallics, two different oxidation states of Pd (0) and Pd (II) were observed. The peaks in 5 wt% bio-Pd/Pt produced by *B. benzeovorans* appeared at 335.23 eV and 337.69 eV and at binding energies of 335.55 eV and 337.42 eV (Fig. 4a) in *D. desulfuricans* (Fig. 4c) respectively. The Pd peaks around 335.23 eV, 335.55 eV, can be assigned to zero-valent Pd [54,55] while the chemical state Pd (II) can be attributed to the peaks at 337.69 eV and 337.42 eV respectively [56] (Table 3a) and may be due to incomplete reduction or oxidation of metallic Pd during sample preparation consistent with the finding of Deplanche et al. [42] for Pd/Au bimetallic synthesis. The 20 wt% bio-Pd/Pt also shows zero-valent Pd peaks at 335.72 eV and 335.17 eV and peaks for Pd (II) at 337.62 eV and 337.26 eV for both Bb (Fig. 4e) and Dd (Fig. 4g) material respectively (Table 3a). The shifts observed in the binding energies of the Pd (0) between the 5 wt% and 20 wt% bio-Pd/Pd of Bb compared to Dd may be due to differences in the surface properties of both bacteria (see Supplementary Table S1) as the cells interact to stabilize Pd NPs.

Considering the binding energies of Pt 4f in both types of cell, the binding energies of the 5 wt% bio-Pd/Pt were below detection

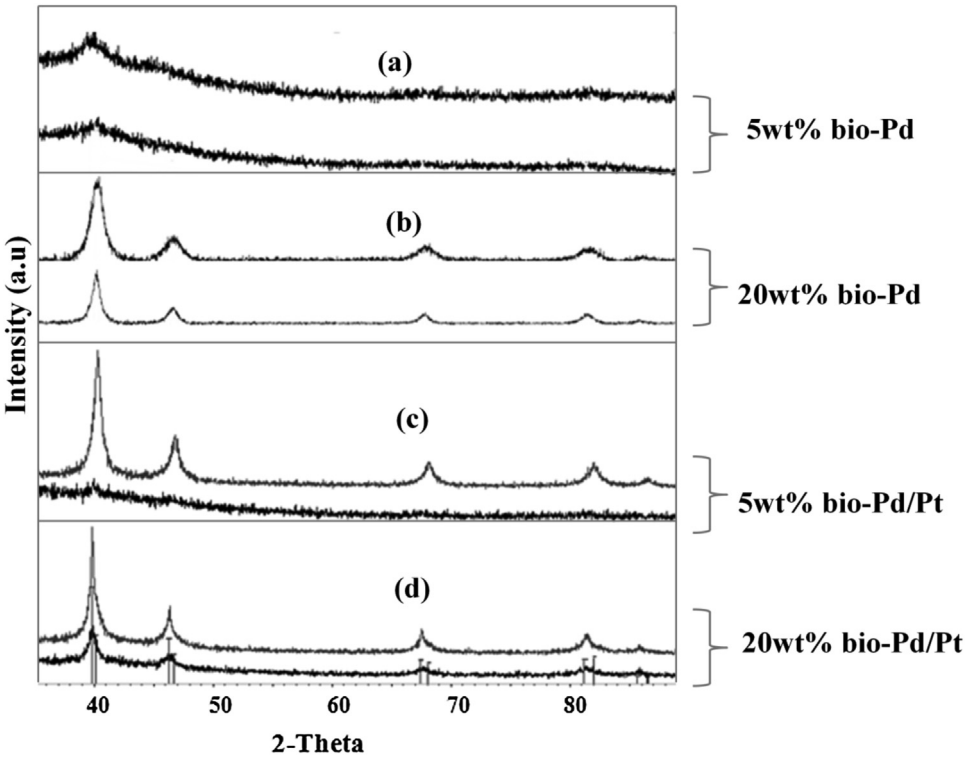


**Fig. 3.** XRD powder patterns of a set of sequence of bio-NPs made by *B. benzeovorans* (top pattern) and *D. desulfuricans* (bottom pattern). In the bimetallic bio-NPs only, the vertical line (right) represents Pt peak position while the vertical line (left) is the Pd peak position.

which appears to have been covered by Pd (Table 3a, Fig. 4b,d) whereas for the 20 wt% bio-Pd/Pt, the binding energies from 71 to 72 eV can be assigned to Pt (0) [57] in the bio-NPs made by both cells (Table 3a). The appearance of these binding energies of Pt in the 20 wt% bio-Pd/Pt NPs (Fig. 4f,h) may be due to the higher metal loading which favours an increase in electron density [55] around Pd as the addition of Pt withdraws electrons from the Pd to be reduced to Pt (0) during the sequential reduction of the bio-NPs as suggested by the observation of Pd (II) (above). The peaks representative of higher binding energies (74–76 eV) may be as a result of the formation of Pt (II), $PtO_2$ or Pt $(OH)_4$ from Pt (IV) species [58]. It can be concluded that Pt exists primarily in the bio-NPs as Pt (0). This interaction suggests the existence of Pd/Pt bimetallic on the surface of the bio-NPs. The presence of Pt (0) in the bimetallic may have generated some residual Pd (II) at the end of the reduction process, characteristic of the binding energies seen above or this may have been 'biosorbed' Pd (II) that was not reduced to Pd (0) 'seeds'.

Table 3b and supplementary Tables S1 and S2 and Fig. S3 show that the bacterial cell surfaces also contain C, N, O and P which can be attributed to carboxyl, amine, hydroxyl and phosphoryl groups found as organic components [59] around the bio-NPs with varying binding energies. These components are responsible for stabilizing [60] the bio-NPs against agglomeration. Table S1 also shows the various molar ratios of the bio-NPs to total carbon. It was observed that the bio-NPs produced by *Bacillus* contain a higher molar ratio of each elemental component (N, P and O) to total carbon than *D. desulfuricans*. It is likely that the elemental ratios in supplementary Table S1 reflect that the probe is detecting the thick layer of peptidoglycan (crosslinked chains of *n*-acetyl glucosamine and *n*-acetyl muramic acid) and teichoic acids on the outer surface of *Bacillus* and peptidoglycan in the periplasm in *Desulfovibrio*, together with the Gram-negative cell outer membrane components of the latter. A detailed study on the mechanism of binding of precious metal species to the two bacterial cell surfaces will be reported elsewhere.

Notably, the O1s of the bimetallic bio-NPs (5 wt% and 20 wt%) produced by the two bacteria have a similar binding energy around 532 eV [54]. However, looking at the 5 wt% bimetallic NPs, they have a binding energy of approximately 531 eV which could be attributed to the interaction of the bacterial surfaces with the NPs due to oxygen from phosphate groups and amide functions [61]. The shift of the O1s peaks to a lower binding energy of around 530 eV observed in bio-NPs with 20 wt% metal loading could be attributed to the formation of metal oxides of Pd and Pt [62,63] on both bacteria. In conclusion, the various surfaces of the bimetallic NPs are mainly covered with Pd and Pt metallic states and could be Pd/Pt core-shell structures, but this requires further verification. Using a similar approach of sequential synthesis, Flynn and Gewirth [64] chemically synthesised Au/Pt core-shell nanoparticles, while Deplanche et al. [42] showed a similar biogenesis and, should a Pd/Pt bimetallic be found potentially useful a more detailed evaluation of the structure of the bio-catalyst would be warranted.

### 3.2. Comparison of bio-Pd/Pt as catalyst for heavy oil upgrading

The cracking of heavy oil involves breaking of C—C, C—H, and C-heteroatom bonds as it is exposed to elevated temperatures. This reaction produces upgraded oil, together with non-condensable gases (*e.g.*, $nC_1$-$C_5$, $iC_4$-$C_5$, olefin $C_2$-$C_4$, $H_2$, $H_2S$, CO and $CO_2$) and coke.

#### 3.2.1. Coke determination

It has been reported that a major cause of catalyst deactivation in heavy oil upgrading is the formation of fouling deposits of "coke" *i.e.* solid or carbonaceous materials that arise due to side reactions that occur on the catalyst surface [65]. An estimate of coke deposition can be made by thermogravimetric analysis (*i.e.* progressive weight loss on heating) of materials before and after reaction. Residual asphaltene, catalysts and other deposits were separated from the reaction as described in materials and methods.

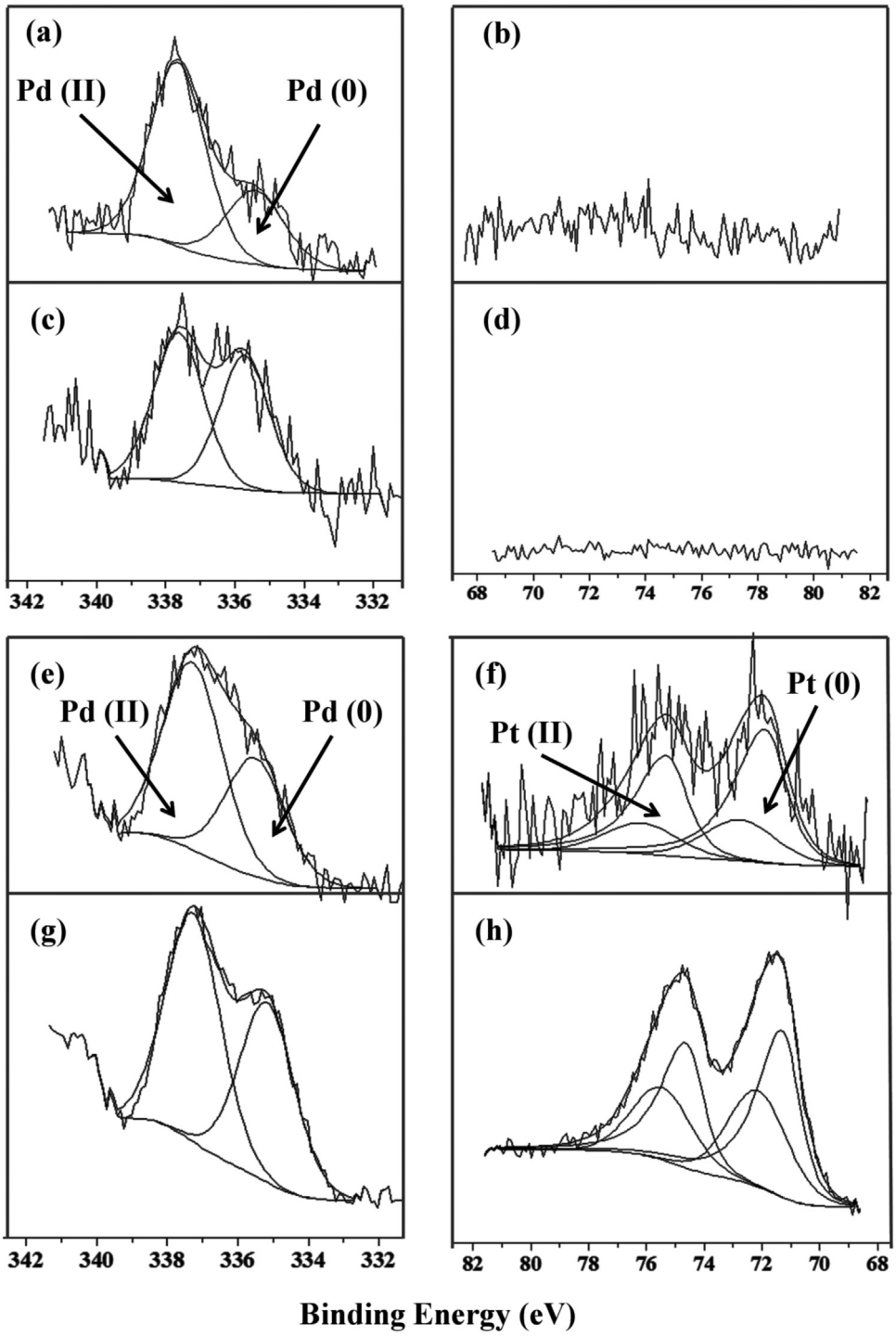


**Fig. 4.** XPS spectra of Pd $3d_{5/2}$ and Pt 4f peaks in 5% bimetallic Pd/Pt bio-NPs made by *B. benzeovorans* (a) and (b); *D. desulfuricans* (c) and (d) and 20% bimetallic Pd/Pt bio-NPs made by *B. benzeovorans* (e) and (f); *D. desulfuricans* (g) and (h) respectively. Fitting was done using Shirley backgrounds, mixed Gaussian-Lorentzian (Voigt) lineshapes.

The percentage of the deposit after reactions that comprises coke was determined using the thermogravimetric (TG) analyser, as the material burnt-off beyond that of *n*-heptane separated asphaltene. Fig. 5 shows the thermograms or weight loss curves as a function of ramp temperature for *n*-heptane-separated asphaltene, fresh Ni-Mo/$Al_2O_3$ and deposit after reaction with Ni-Mo/$Al_2O_3$ (Fig. 5a) and also the metal-unsupplemented bacterial cells, fresh bio-NPs and the deposits after reaction with *D. desulfuricans* (Fig. 5b) and *B. benzeovorans* (Fig. 5c).

The fresh 5 and 20 wt% bio-catalysts (Pd or Pd/Pt) lost 65 wt.% of their masses during the temperature rise to 550 °C in air. This is as a result of moisture removal (from 25 to 80 °C), charring of the biomass (80–300 °C) and subsequent burn-off of the formed carbon (from 300 to 550 °C). The thermogram curves of the air-dried bacterial cells decorated with Pd or Pd/Pt NPs (*i.e.*, fresh bionanparticles) show that the residual mass ranged from 8.7–13 wt% (5 wt% Pd and 5 wt%Pd/Pt) and 20.6–27.7 wt% (20% Pd and 20%Pd/Pt). Most of the residual masses were metals (*i.e.*, Pd or Pd/Pt) with little biomass char formed, which accounts for about 4 wt% from the TGA

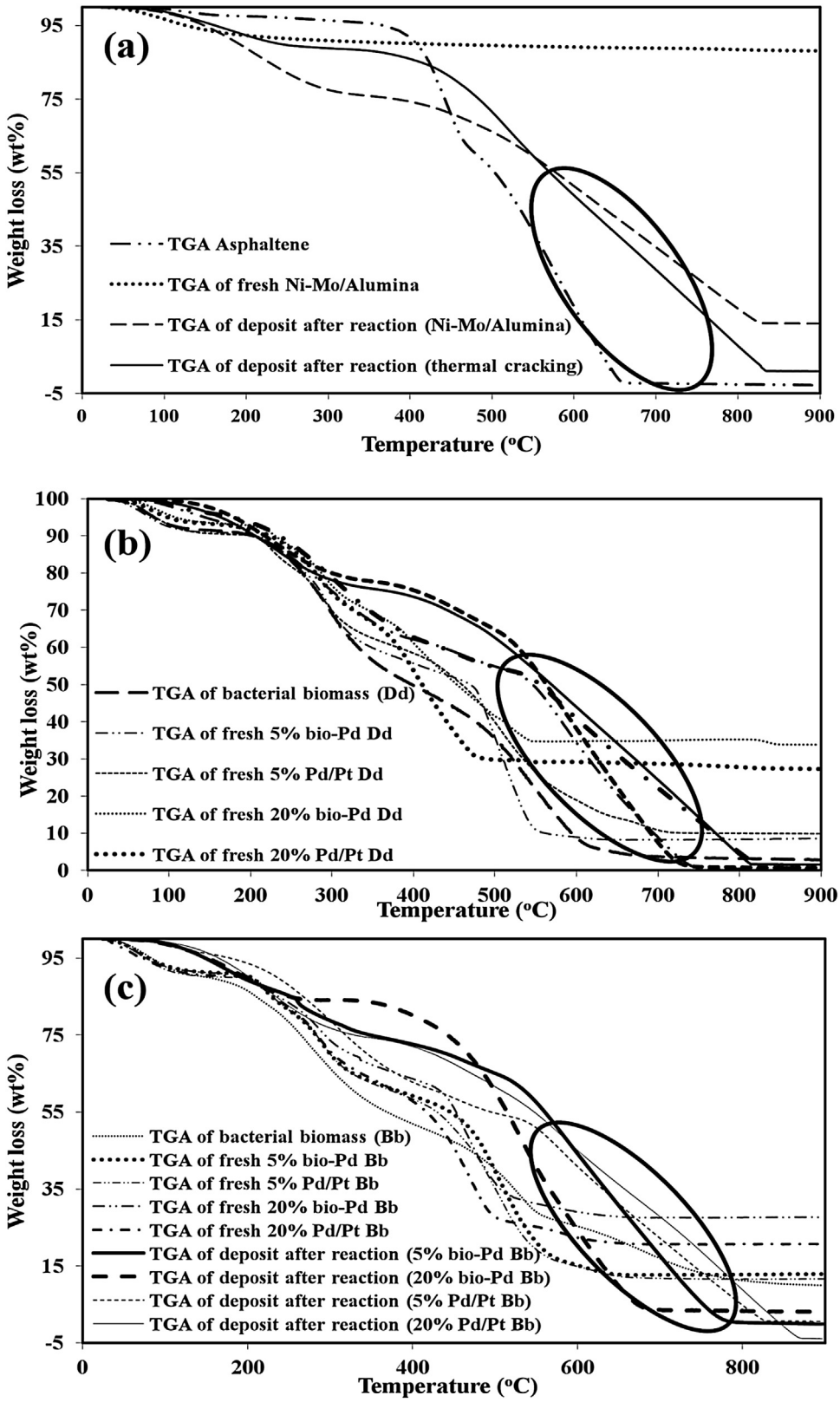


**Fig. 5.** TGA curves of fresh bio-Pd and Pd/Pt, *n*-heptane separated asphaltene, and deposits after reactions at 425 °C, 500 rpm, and 30 min reaction time. Circled regions: responses attributed to coke and residual catalyst.

of the bacterial cells without metals (Fig. 5b,c). There was a complete burn-off of the separated asphaltenes using *n*-heptane as the temperature increased from 430 to 600 °C. Therefore, the burn-off above 600 °C (Fig. 5a) for the deposit after reaction is attributed to rejected coke after upgrading [66]. Hence, from the weight loss curves of deposits after reaction the residues after burn-off from 600 to 820 °C was coke. (Fig. 5a–c). The weight loss from 25 to 100 °C for the fresh 19.2 wt% Ni-Mo/$Al_2O_3$ represents the removal

**Table 4**
Mass balance of liquid (*i.e.*, light oil), gas and coke yields after reaction.

| Experiments | Liquid (wt%) | | Gas (wt%) | | Coke (wt%) | |
|---|---|---|---|---|---|---|
| | Bb | Dd | Bb | Dd | Bb | Dd |
| Thermal | 79.83 ± 1.6 | | 10.02 ± 1.2 | | 10.15 ± 2.0 | |
| Biomass alone | 84.86 ± 1.1 | 82.64 ± 0.0 | 8.51 ± 0.8 | 9.72 ± 0.0 | 6.63 ± 1.3 | 7.64 ± 0.0 |
| 5 wt% bio-Pd | 89.32 ± 0.4 | 89.09 ± 0.2 | 7.48 ± 0.2 | 7.62 ± 0.2 | 3.20 ± 0.4 | 3.30 ± 0.1 |
| 20 wt% bio-Pd | 89.45 ± 0.7 | 89.80 ± 0.4 | 7.61 ± 0.1 | 7.04 ± 0.4 | 2.94 ± 0.1 | 3.16 ± 0.5 |
| 5 wt%bio-Pd/Pt | 89.20 ± 0.3 | 89.40 ± 0.5 | 7.07 ± 0.2 | 6.73 ± 1.1 | 3.73 ± 0.2 | 3.87 ± 0.2 |
| 20 wt%bio-Pd/Pt | 89.02 ± 0.5 | 89.13 ± 0.3 | 6.78 ± 0.1 | 6.80 ± 0.2 | 4.20 ± 0.2 | 4.07 ± 0.6 |
| Commercial catalyst | 87.25 ± 0.5 | | 7.73 ± 0.7 | | 5.02 ± 0.8 | |

*Note:* Bb = *B. benzeovorans;* Dd = *D. desulfuricans*; Commercial catalyst = Ni-Mo/$Al_2O_3$.

of moisture; beyond this temperature (100 °C) the catalyst is thermally stable. However, 41.3% of the deposit after reaction with Ni-Mo/$Al_2O_3$ particles was coke (Fig. 5a). At 425 °C and 500 rpm experimental condition the bacterial biomass would have been destroyed releasing the Pd or Pd/Pt NPs into the reaction medium. However, the Pd or Pd/Pt NPs mass used in the experiments were so low (*i.e.*, 1 mg NPs/g oil = 0.1 wt.% NPs), that any mass changes to the Pd or Pd/Pt NPs as result of modification during the TGA would be negligible compared to the weight loss due to coke burn-off. Consequently, any biochar retained in the carbonaceous deposit after reaction will be burnt-off from 300 to 550 °C during the TGA which is prior to the start of the coke burn-off at 600 °C (Fig. 5). The coke content of the deposits after reaction with 5 wt% (Pd or Pd/Pt) on bacterial cells ranged from 25 to 29.2 wt.% while that of 20 wt% ranged from 20.2 to 38.1 wt% (Fig. 5b,c). The coke content of the deposit after reaction ranges from 20 to 43 wt.% of amount of deposit. The deposit after reaction with particles of Ni-Mo/$Al_2O_3$ showed a higher coke content and burn-off temperature (about 820 °C) compared to those of bio-NPs (750–800 °C). This high burn-off temperature can be attributed to the hardness of the produced coke resulting from the acidity of the alumina support [66]. The coke deposits for the samples are shown in Table 4, from which it can be concluded that thermal cracking and metal-free biomass, followed by commercial catalyst, produced more coke than the bio-NPs.The yields of light oil (*i.e.* liquid), gas and coke after upgrading with thermal cracking, biomass alone, commercial catalyst and bionanoparticles are shown in Table 4.

Table 4 shows that the coke yield was decreased significantly after reaction with 5 wt.% and 20 wt.% bionanoparticles of Pd and Pd/Pt promoted catalysts. Although there is no significant difference ($P > 0.05$) between the NPs made by the two bacteria at 0.05 significance level (except for 20 wt.% bio-Pd: $P = 0.004$) the bionanoparticles displayed significant effects in suppressing coke formation compared to thermal cracking (10.15 wt.% of coke) and commercial catalyst (5.02 wt.%) while biomass alone yielded 6.63 wt.% for Bb and 7.64 wt.% for Dd of coke respectively. The biomass is 'seen' by the reaction as additional carbon-based material as it would be pyrolyzed during the reaction.

Analysis of the produced gas during heavy oil upgrading has shown that hydrogen is produced [50], *e.g.* 20 mol% hydrogen was found in the produced gas from an *in situ* combustion pilot at Marguerite Lake, Alberta, Canada [67] and subsequently Hart et al. [49] found 1.5 to 2.5 vol.% hydrogen in the produced gas after the use of dispersed ultrafine Co-Mo/$Al_2O_3$ catalyst upgrading of heavy oil in a batch reactor. It is well known that metals perform a hydroconversion function; hence this observation may be explained by the fact that the produced hydrogen gas molecules, which are readily adsorbed onto the surfaces of nanoparticles, could be dissociated to produce reactive hydrogen species which subsequently react with the cracked intermediates to produce stable lower molecular weight products. Correspondingly, the increased yield of coke resulted in a decreased yield of the desired liquid product [67,68]. On the other hand, thermal cracking without catalyst has shown a greater tendency to form coke due to free radical addition polymerisation reaction [49].

Table 4 shows that the nanoparticles of Ni-Mo/$Al_2O_3$ hydrodesulfurization (HDS) catalyst yielded higher coke than bio-NPs. This is attributable to a cracking function provided by the alumina acidic support which increases the cracking reaction leading to more coke formation [69] unlike the bio-NPs that are well dispersed and stabilized by various functional groups on the neutral bacterial support [60] (see above).

For all bionanoparticles of Pd or Pd/Pt catalysts, the amount of gaseous hydrocarbon produced was lower than that of the thermal cracking and the biomass-promoted reaction with no metal NPs (Table 4). A typical composition of the produced gas has been reported elsewhere [12,50]. The presence of nanoparticles suppresses gas formation probably as a result of the transfer of active hydrogen, methyl and ethyl radical additions *via* the NPs to stabilise hydrocarbon radicals formed by thermal cracking into the liquid phase [70]. A similar observation of a lower yield of gas was reported by Hossain et al. [41] for a synergistic effect of Pd/Rh promoted Co/HPS [cobalt decorated with high porous saponite (clay)] catalyst for upgrading of vacuum gas oil at 400 °C in a batch autoclave reactor. These results are expected because of the availability of reactive hydrogen due to hydrogen spillover *i.e.* the dissociation and chemisorption/physisorption of hydrogen atoms/molecules on metals such as Pd, Pt, Ni, Mo, *etc.*, followed by incorporation of the active hydrogen onto the nearest receptor [71] which, in this case, could be attack on biomass components, introduced by the nanoparticles that helps to suppress the formation of lighter gases and coke [41]. Hence, the over cracking of produced hydrocarbon intermediates leading to undesirable light gaseous products is inhibited. This conclusion can be reinforced by the high yield of gas in thermal cracking and upgrading with biomass only. Hence, the bimetallic bioNPs may have enhanced hydrogen, methyl and ethyl transfer because of the synergistic effect of Pd/Pt and their 'biochemical' environment to stabilise cracked fragments of heavy oil molecules. In this manner, the formation of large molecular weight hydrocarbons as a result of free radical addition reactions would be significantly suppressed. All metallised samples gave a higher proportion of liquid post-reaction than either thermal cracking or biomass alone (Table 4).

In summary, the performance of the catalyst on the two types of bio-support was similar overall (within experimental error) with no major differences between bio-Pd and the bimetallics (Table 4) although 20 wt% bio Pd/Pt produced more coke than 20 wt% bio-Pd alone, whereas at 5 wt% loadings they were similar. The lower gas production by the 20 wt% bimetallic could be attributed to more gas being consumed into unwanted side reactions.

### 3.2.2. API gravity and viscosity

API (American Petroleum Institute) gravity is a standard parameter that determines the transportability of crude oil *via* pipelines

**Table 5**
Produced oil API gravity increment and viscosity after reaction (feed oil: 13.8 °API and 1031 mPa s).

| Experiments | API gravity increments (°) | | Viscosity (mPa s) | |
|---|---|---|---|---|
| | Bb | Dd | Bb | Dd |
| Thermal | 6.3 ± 0.3 | | 13.8 ± 0.4 | |
| Biomass alone | 6.1 ± 0.5 | 6.2 ± 0.0 | 16.0 ± 2.2 | 14.8 ± 0.0 |
| 5 wt% bio-Pd | 7.8 ± 0.3 | 7.8 ± 0.2 | 9.7 ± 0.6 | 8.1 ± 0.4 |
| 20 wt% bio-Pd | 7.4 ± 0.4 | 7.5 ± 0.2 | 8.8 ± 0.7 | 10.7 ± 2.5 |
| 5 wt% bio-Pd/Pt | 9.1 ± 0.4 | 9.6 ± 0.8 | 7.0 ± 0.3 | 5.8 ± 0.6 |
| 20 wt% bio-Pd/Pt | 9.2 ± 0.9 | 8.4 ± 0.6 | 7.4 ± 1.2 | 6.2 ± 0.7 |
| Commercial catalyst | 11.1 ± 0.3 | | 3.7 ± 0.6 | |

*Note:* Bb = *B. benzeovorans;* Dd = *D. desulfuricans;* Commercial catalyst = Ni-Mo/$Al_2O_3$.

[72]. For heavy oil to be transported, the viscosity must be reduced and lower than 250 mPa s at 37.8 °C [73]. The viscosity and API gravity of heavy oil depends to a large extent on its macromolecular weight constituents such as resins and asphaltenes. It is well known that hydrocarbons with larger weight and high boiling point exhibit high density and viscosity. Table 5 shows the API gravity increments and viscosities of produced oil samples after reaction with thermal cracking, biomass alone, bio-supported NPs of Pd or Pd/Pt, and NPs of Ni-Mo/$Al_2O_3$. The oil produced by thermal cracking had a lower API gravity increment and higher viscosity compared to the produced oil samples after reaction with any of the catalyst. Moreover, the produced oils after upgrading with bimetallic NPs (Pd/Pt) had approximately 2° further increase in API gravity compared to those upgraded with monometallic Pd (~7.6 °API on average). The values of viscosity after upgrading therefore can be summarised as follows: 13.8 mPa s (thermal), 8.1 mPa s (bioNPs) and 3.7 mPa s (nanoparticles of Ni-Mo/$Al_2O_3$) relative to 1031 mPa s for the feed heavy oil that was subjected to the THAI process prior to use in these experiments. This level of viscosity reduction would improve production and pipeline transport with respect to the feed oil. A similar level of viscosity reduction of 98.9% for Liaohe extra-heavy oil using nano-nickel catalyst in batch reactor has been reported [74]. While, for small quantities, the small improvement given by catalytic augmentation is questionable, the beneficial effects at scale and overall process economics, awaits evaluation. Overall, the use of the mixed Pd/Pt catalyst offers some benefit as compared to bio-Pd (Table 5) which justifies future investigations into the use of catalyst biorefined from waste; although the benefit is small at this scale it would translate to a large advantage at full process scale.

The thermal reaction involves cracking of C—C and C-heteroatom bonds, cracking of side chains from aromatics and asphaltenes, aromatization of aliphatic structures, and condensation of aromatic radicals to form coke. Hence, generated fragments commonly undergo addition reaction to larger molecular weight species which adversely impacts on the produced oil API gravity and viscosity after upgrading by thermal cracking. In a catalytic environment, the presence of metals such as Pd and Pt are thought to activate hydrogen-transfer reactions from C—H bond cleavage to cap some of the produced radicals [49,50,68], thereby narrowing the molecular weight of the product compared to thermal cracking alone (see later).

An industrial hydrodesulfurization (HDS) Ni-Mo/γ$Al_2O_3$ catalyst was also evaluated under the same reaction conditions and the activity of this catalyst was also included for comparison purposes. This produced better upgrading than the bio-catalysts (Table 5) but correspondingly more coke (Table 4) instead of the dual benefit obtained by using the biomaterials. Comparing the extent of upgrading by Pd/Pt/bio-NPs and Ni-Mo/$Al_2O_3$, the produced oil API gravity for the bio-derived and commercial catalysts was 9.6° (Pd/Pt 5 wt.%) and 11.1° (19.2 wt% Ni-Mo/$Al_2O_3$) respectively. The ~1.5°API increment obtained with the commercial HDS Ni-Mo catalyst can be attributed to the additional cracking role of acid sites of the alumina support whereas bio-nanoparticles of Pd/Pt lack such sites although immobilization of catalyst on alumina support is entirely feasible *via* a self-adhering biofilm [75,76]; the extent of continued bio-adhesion to support under, effectively, pyrolysis conditions is not known but co-delivery of alumina and bio-components would be achieved and may prove advantageous. However, the alumina support would lack the potential sites for amelioration of the coking problem; the bio-Pd/Pt is superior to the commercial catalyst in this regard. Macromolecules such as resins and asphaltenes are known coke precursors because of their high aromaticity, molecular weight, and heteroatom content. These components confer the characteristic low API gravity, high viscosity and low yield of light distillates with lower boiling points upon distillation. The higher API gravity observed after upgrading therefore indicates that the produced oil composition has shifted towards lighter components with lower molecular weight (but still accompanied with polymerization and condensation of some of the macromolecules to form coke). Heavy oil is known to be hydrogen-deficient, thus coke formation can be suppressed remarkably if hydrogen/hydrogen-donor is available to stabilize generated free radicals during reaction [51,69]. In this respect the well known property of Pd (0) to hold $H_2$ within its lattice may help transfer hydrogen into the reaction [77]. Other authors showed that Pd nanocrystals covered with a metal-organic framework have twice the hydrogen storage capacity as compared to bare Pd nanocrystals [77].

### 3.2.3. True boiling point (TBP) distribution

The crude oil boiling point distribution curve is an important yardstick of quality evaluation and refinery process design. It has been reported that aliphatic-rich oil generally has a higher API gravity and high yield of fuel distillates than aromatic-rich oils [78]. Additionally, a high content of sulfur, metals and nitrogen-containing compounds of the heavy oil adds to their low API gravity and low fuel distillate yields [66]. The true boiling point (TBP) distribution curves for the feed and produced oils after reaction with the different bio-NPs and thermal cracking are shown in Fig. 6. The shift of the TBP distribution curves of the produced oils after reaction to the left of TBP curve of the feed oil is an indication of the extent of upgrading achieved, representing the extent of conversion of heavy molecular weight compounds into low-boiling fractions.

The performance of the bioNPs was evaluated in comparison to the control experiments such as the feed heavy oil, upgraded oil by thermal cracking, and upgraded oil with biomass only (without metals), with the upgraded oils with bioNPs of Pd and Pd/Pt all subjected to the same operating conditions.

Fig. 6 shows that oil upgrading with the addition of bionanoparticles of Pd and Pd/Pt favours a significant shift towards lighter distillate fractions in comparison to thermal cracking, upgrading with biomass only (no metal nanoparticles) and the feed oil reference. A 53 and 65 °C shift to the left in the boiling point axis at 50 vol.% yield can be observed for thermal cracking and with biomass only in comparison to the feed oil TBP curve. This rose to 90 °C (5 wt.% $Pd_{Bb}$), 94 °C (20 wt.% Pd/$Pt_{Bb}$) and 96 °C (20 & 5 wt.% Pd/$Pt_{Dd}$ and 5 wt.% Pd/$Pt_{Bb}$) but only 73 °C (20 wt.% $Pd_{Bb}$ and 20 wt $Pd_{Dd}$) at 50 vol.% yield after the reactions using Pd and Pd/Pt/bio-NPs. This shift in temperature to the left of the TBP curve of the feed oil can be attributed to the increased amount of low-boiling fractions in the upgraded oil samples after reaction with metallic bionanoparticles. An important observation is made with the use of commercial Ni-Mo/Alumina catalyst and 5 w% bio-Pd/Pt of both bacteria, as the shift towards lower distillable temperatures is comparable.

Overall, little difference was seen in the use of Pd-only and Pd/Pt bimetallic bio-catalysts which has implications for the future biofabrication of catalysts using PGM waste sources. Such 'green'

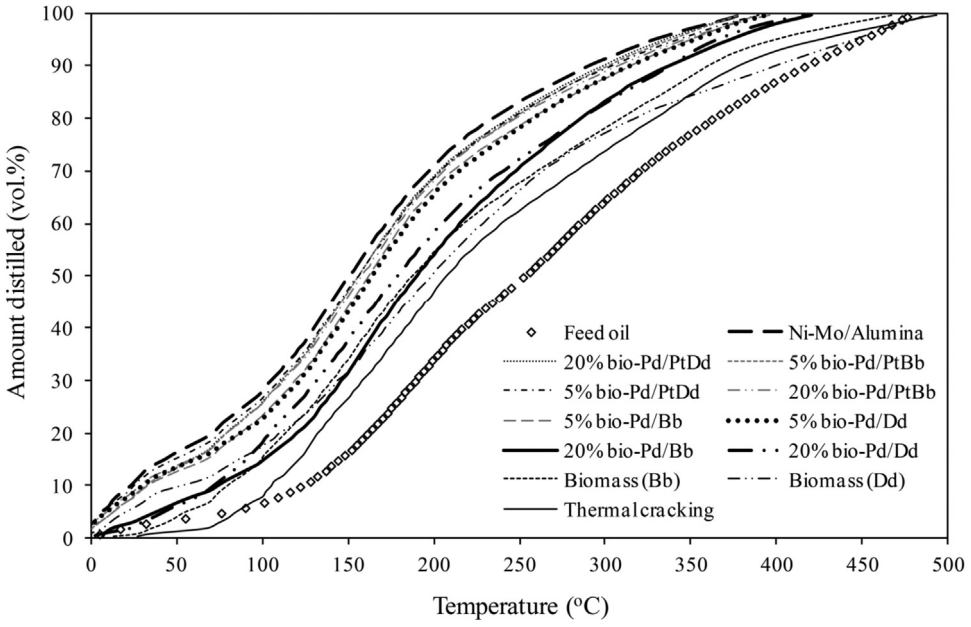


**Fig. 6.** Simulated distillation curves of feed and produced oils after reaction with the different nanoparticles at temperature 425 °C, agitation 500 rpm, metal NP-to-oil ratio 1 (mg/g), initial pressure 20 bar and 30 min reaction time.

fabrication for catalyst synthesis from road dusts for this application in heavy oil upgrading has been reported in preliminary studies [29,79] and will be described in full in later publications.

## 4. Conclusions and future scope

This study shows the use of bio-NPs made by cells of Gram-positive (*B. benzeovorans*) and Gram-negative (*D. desulfuricans*) bacteria in heavy oil upgrading. The bio-NPs of Pd and Pd/Pt were better catalysts as they suppressed coke formation when compared to using non-metallised biomass, a thermal non-catalytic process and NPs of commercial catalyst of Ni-Mo/$Al_2O_3$, and they also produced more volumes of liquid fractions on average. The API gravity produced by commercial catalyst, Ni-Mo/$Al_2O_3$ was higher but hindered by coking when compared with the bio-NPs. There was generally no significant difference in terms of the catalytic behaviour of the bio-NPs made by the two bacteria, *B. benzeovorans* would be considered a better platform of choice in catalytic synthesis, as *Baccillus* spp. are easier to produce at scale (and already are grown thus to make enzymes at industrial-scale) than by using the slower growing, obligately anaerobic, *D. desulfuricans*. The differences in the bioentities (particle size *via* XRD and TEM and elemental surface composition *via* XPS analysis) make little difference to the outcome of heavy oil upgrading.

## Notes

The authors declare no competing financial interests.

## Acknowledgements

The authors acknowledge, with thanks, financial support from a Commonwealth scholarship of the United Kingdom to JBO. The project was also supported by EPSRC (grant number EP/J008303/1) to JW and LEM and NERC (grant number NE/L014076/1). The Science City Photoemission Facility used in this research was funded through the Science Cities Advanced Materials Project 1: Creating and Characterising Next Generation of Advanced Materials with support from AWM and ERDF funds

## Appendix A. Supplementary data

Supplementary data associated with this article can be found, in the online version, at http://dx.doi.org/10.1016/j.apcatb.2016.10.074.

## References

[1] US Energy Information Administration (EIA): International Energy Outlook. Report number: Doe/EIS-0484. Sep. 9th, 2014.
[2] BP Statistical review of world energy. June, 2014.
[3] World Energy Outlook, International Energy Agency (IEA), ISBN: 978 9264 12413 4. November, 2014.
[4] Total Oil and Gas. Reserves for the future. http://www.total.com/en/energies-expertise/oil-gas/exploration-production/strategic-sectors/heavy-oil/challenges/reserves-future. (Accessed online 05.05.15).
[5] M.F.M. de Sena, L.P. Rosa, A. Szklo, Energy Policy 61 (2013) 51–59.
[6] J.W. Buza, An Overview of Heavy Oil Carbonate Reservoirs in the Middle East. Search and Discovery Article #10277. http://www.searchanddiscovery.com/documents/2010/10277buza/ndx_buza.pdf, 2010.
[7] I.M. Head, D.M. Jones, S.R. Larter, Nature 426 (2003) 344–352.
[8] A.Y. Huc, Geological origin of heavy oil, in: Alain-Yves Huc (Ed.), Heavy Crude Oil: From Geology to Upgrading. An overview, Technip, Paris, 2011, pp. 25–31, ISBN 978-2-7108-0890-9.
[9] J.P. Heraud, A. Kamp, J.F. Argiller, In-situ upgrading of heavy oil and Bitumen, in: Alain-Yves Huc (Ed.), Heavy Crude Oil: From Geology to Upgrading. An Overview, Technip, Paris, 2011, pp. 388–402, ISBN978-2-7108-0890-9.
[10] L.C. Castaneda, J.A.D. Munoz, J. Ancheyta, Catal. Today 220 (2014) 248–273.
[11] M. Greaves, A. El-Saghr, T.X. Xia, Prepr. ACS Div. Pet. Chem. 47 (2000) 595–598.
[12] A. Hart, G. Leeke, M. Greaves, J. Wood, Energy Fuels 28 (2014) 1811–1819.
[13] M. Greaves, T.X. Xia, J. Can. Petrol. Technol. 43 (2004) 25–30.
[14] K. Deplanche, A. Murray, S. Taylor, L.E. Macaskie, Biorecycling of precious metals and rare earth elements, in: M.M. Rahman (Ed.), Nanomaterials, In Tech publishing, Rijeka, Croatia, 2011, pp. 279–314 (ISBN: 978-953-307-913-4).
[15] A.N. Mabbett, D. Sanyahumbi, P. Yong, L.E. Macaskie, Environ. Sci. Technol. 40 (2006) 1015–1021.
[16] K.B. Narayanan, N. Sakthivel, Adv. Colloid Interface Sci. 156 (2010) 1–13.
[17] P. Yong, I.P. Mikheenko, K. Deplanche, M.D. Redwood, L.E. Macaskie, Biotechnol. Lett. 32 (2010) 1821–1828.
[18] R.L. Orozco, M.D. Redwood, P. Yong, I. Caldelari, F. Sargent, L.E. Macaskie, Biotechnol. Lett. 32 (2010) 1837–1845.
[19] A.J. Murray, Platinum group metal recovery from powdery wastes. Patent No EP2411660A1; PCT/GB2010/00052, 2012.
[20] A.J. Murray, PhD Thesis, University of Birmingham, 2012.
[21] A. Hart, J.B. Omajali, A.J. Murray, L.E. Macaskie, M. Greaves, J. Wood, Fuel 180 (2016) 367–376.

[22] S. Selenska-Pobell, P. Panak, V. Miteva, I. Boudakov, G. Bernhard, H. Nitsche, FEMS Microbiol. Ecol. 29 (1999) 59–67.
[23] J.M. Foulkes, K.J. Malone, V.S. Coker, N.J. Turner, J.R. Lloyd, ACS Catal. 11 (2011) 1589–1594.
[24] K. Deplanche, J.A. Bennett, I.P. Mikheenko, J. Omajali, A.S. Wells, R.E. Meadows, J. Wood, L.E. Macaskie, Appl. Catal. B 147 (2014) 651–665.
[25] H. Ortiz-Moreno, J. Ramírez, F. Sanchez-Minero, R. Cuevas, J. Ancheyta, Fuel 130 (2014) 263–272.
[26] J.K. Dunleavy, Platinium Met. Rev. 50 (2006) 110.
[27] Y.J. Tong, Chem. Soc. Rev. 41 (2012) 8195–8209.
[28] A.J. McCue, J.A. Anderson, Catal. Sci. Technol. 4 (2014) 272–294.
[29] J.B. Omajali, Ph.D. Thesis, University of Birmingham, 2015.
[30] J.B. Omajali, I.P. Mikheenko, M.L. Merroun, J. Wood, L.E. Macaskie, J. Nanopart. Res. 17 (2015) 1–17.
[31] N.J. Creamer, I.P. Mikheenko, P. Yong, K. Deplanche, D. Sanyahumbi, J. Wood, K. Pollmann, M. Merroun, S. Selenska-Pobell, L.E. Macaskie, Novel supported Pd hydrogenation bionanocatalyst for hybrid homogeneous/heterogeneous catalysis, Catal. Today 128 (2007) 80–87.
[32] J.A. Bennett, I.P. Mikheenko, K. Deplanche, I.J. Shannon, J. Wood, L.E. Macaskie, Appl. Catal. B 140–141 (2013) 700–707.
[33] V.S. Baxter-Plant, I.P. Mikheenko, L.E. Macaskie, Biodegradation 14 (2003) 83–90.
[34] M.D. Redwood, K. Deplanche, V.S. Baxter-Plant, L.E. Macaskie, Biotechnol. Bioeng. 99 (2008) 1045–1054.
[35] A.N. Mabbett, P. Yong, J.P.G. Farr, L.E. Macaskie, Biotechnol. Bioeng. 87 (2004) 104–109.
[36] S. De Corte, T. Sabbe, T. Hennebel, L. Vanhaecke, B. De Gusseme, W. Verstraete, N. Boon, Water Res. 46 (2012) 2718–2726.
[37] J. Zhu, J. Wood, K. Deplanche, I. Mikheenko, L.E. Macaskie, Appl. Catal. B 199 (2016) 108–122.
[38] H.L. Parker, E.L. Rylott, A.J. Hunt, J.R. Dodson, A.F. Taylor, et al., PLoS One 9 (2014) e87192, http://dx.doi.org/10.1371/journal.pone.0087192.
[39] K.B. Narayanan, N. Sakthivel, Adv. Colloid Interface Sci. 169 (2011) 59–79.
[40] A. Bunschoten, P.T.K. Chin, T. Buckle, M. van der Linden, A. Barendregt, M.A. Verheijen, F.W.B. van Leeuwen, Eur. J. Inorg. Chem. 18 (2016) 3030–3035.
[41] M.M. Hossain, M.A. Al-Saleh Shalabi, T. Kimura, T. Inui, Appl. Catal. A 278 (2004) 65–71.
[42] K. Deplanche, M.L. Merroun, M. Casadesus, D.T. Tran, I.P. Mikheenko, J.A. Bennett, J. Zhu, I.P. Jones, G.A. Attard, J. Wood, S. Selenska-Pobell, L.E. Macaskie, J.R. Soc, Interface 9 (2012) 1705–1712.
[43] S. Taylor, MPhil Thesis, University of Birmingham, UK, 2012.
[44] K. Deplanche, I. Caldelari, I.P. Mikheenko, F. Sargent, L.E. Macaskie, Microbiology 156 (2010) 2630–2640.
[45] M. Jaboyedoff, B. Kubler, P.H. Thelin, Clay Miner. 34 (1999) 601–617.
[46] N. Fairley, CasaXPS. Casa Software Ltd. www.casaxps.com. 2013.
[47] A. Hart, A. Shah, G. Leeke, M. Greaves, J. Wood Ind. Eng. Chem. Res. 52 (2013) 15394–15406.
[48] A. Shah, R.P. Fishwick, G.A. Leeke, J. Wood, S.P. Rigby, M. Greaves, J. Can. Petrol. Technol. 50 (2011) 33–47.
[49] A. Hart, M. Greaves, J. Wood, Chem. Eng. J. 282 (2015) 213–223.
[50] A. Hart, G. Leeke, M. Greaves, J. Wood, Fuel 119 (2014) 226–235.
[51] C.-M. Lin, T.-L. Hung, Y.-H. Huang, K.-T. Wu, M.-T. Tang, C.-H. Lee, C.T. Chen, Y.Y. Chen, Phys. Rev. B 75 (2007), 125426-1–125426-2.
[52] G.T. Fu, X. Jiang, L.F. Ding, L. Tao, Y. Chen, Y.W. Tang, Y.M. Zhou, S.H. Wei, J. Lin, T.H. Lu, Appl. Catal. B 138 (2013) 167–174.
[53] Y. Chen, B. He, T. Huang, H. Liu, Colloids Surf. A Physicochem. Eng. Asp. 348 (2009) 145–150.
[54] J. Park, S.W. Won, J. Mao, I.S. Kwak, Y.-S. Yun, J. Hazard. Mater. 181 (2010) 794–800.
[55] L. Wu, S. Shafii, M.R. Nordin, K.Y. Liew, J. Li, Mater. Chem. Phys. 137 (2012) 493–498.
[56] M. Hasik, A. Bernasik, A. Drelinkiewicz, K. Kowalski, E. Wenda, J. Camra, Surf. Sci. 507–510 (2002) 916–921.
[57] F. Sen, G. Gokagac, J. Phys. Chem. C 111 (2007) 5715–5720.
[58] Z.Q. Tian, S.P. Jiang, Y.M. Liang, P.K. Shen, J. Phys. Chem. B 110 (2006) 5343–5350.
[59] Y.F. Dufrêne, P.G. Rouxhet, Colloids Surf. B 7 (1996) 271–279.
[60] C. Rodriguez-Navarro, C. Jimenez-Lopez, A. Rodriguez-Navarro, M.T. Gonzalez-Muñoz, M. Geochim, Cosmochim. Acta 71 (2007) 1197–1213.
[61] F. Ahimou, C.J.P. Boonaert, Y. Adriaensen, P. Jacques, P. Thonart, M. Paquot, P.G. Rouxhet, J. Colloid Interface Sci. 309 (2007) 49–55.
[62] J.S. Corneille, J.-W. He, D.W. Goodman, Surf. Sci. 338 (1995) 211–224.
[63] M.C. Biesinger, B.P. Payne, L.W.M. Lau, A. Gerson, R.S.C. Smart, Surf. Interface Anal. 41 (2009) 324–332.
[64] N.T. Flynn, A.A. Gewirth, J. Raman Spectrosc. 33 (2002) 243–251.
[65] P. Forzatti, L. Lietti, Catal. Today 52 (1999) 165–181.
[66] A. Hart, PhD Thesis, University of Birmingham, UK, 2014.
[67] R.J. Hallam, L.E. Hajdo, J.K. Donnelly, R.P. Baron, SPE Reserv. Eng. 4 (1989) 178–186.
[68] A. Zachariah, L. Wang, S.F. Yang, V. Prasad, A. de Klerk, Energy Fuels 27 (2013) 3061–3070.
[69] S. Alkhaldi, M.M. Husein, Energy Fuels 28 (2014) 643–649.
[70] H. Purón, J.L. Pinilla, I. Suelves, M. Millan, Catal. Today 249 (2015) 79–85.
[71] J.H. Guo, H. Zhang, Y.J. Tang, X.L. Cheng, Phys. Chem. Chem. Phys. 15 (2013) 2873–2881.
[72] F. Sánchez-Minero, G. Sánchez-Reyna, J. Ancheyta, G. Marroquin, Fuel 138 (2014) 193–199.
[73] A.P. Szilas (Ed.), Production and Transport of Oil and Gas, Elsevier, Amsterdam, 1975, pp. 1–496.
[74] L. Wei, Z. Jian-hua, Q. Jian-hua, J. Fuel Chem. Technol. 35 (2007) 176–180.
[75] D.A. Beauregard, P. Yong, L.E. Macaskie, M.L. Johns, Biotechnol. Bioeng. 107 (2010) 11–20.
[76] P. Yong, W. Liu, Z. Zhang, D. Beauregard, M.L. Johns, L.E. Macaskie, Biotechnol. Lett. 37 (2015) 2181–2191.
[77] G.Q. Li, H. Kobayashi, J.M. Taylor, R. Ikeda, Y. Kubota, K. Kato, M. Takata, T. Yamamoto, S. Toh, S. Matsumura, H. Kitagawa, Nat. Mater. 13 (2014) 802–806.
[78] X.Y. Chen, J.J. Gao, Y.Z. Lu, H. Meng, C.X. Li, Fuel Process. Technol. 130 (2015) 7–11.
[79] A.J. Murray, J. Omajali, Y. Del Mastio, A. Hart, J. Wood, L.E. Macaskie, Adv. Mater. Res. 1130 (2015) 623–626.